PERIODICUM BIOLOGORUM
VOL. 113, No 4, 417–423, 2011

UDC 57:61
CODEN PDBIAD
ISSN 0031-5362

Original scientific paper

Experimental verification of heat source parameter estimation from 3D thermograms

IVAN SOVIĆ
TOMISLAV LIPIĆ
LUKO GJENERO
IVAN GRUBIŠIĆ
KAROLJ SKALA

Ruđer Bošković Institute
Center for informatics and computing
Bijenička 54, Zagreb, Croatia

Correspondence:
Ivan Sović
Ruđer Bošković Institute
Center for informatics and computing
Bijenička 54, Zagreb, Croatia
E-mail: ivan.sovic@irb.hr

Received November 24, 2011.

Abstract

Major amount of thermal radiation emitted by objects is located in a small part of the infrared spectrum of electromagnetic radiation, called the thermal infrared spectrum, and can be observed and measured using thermal infrared measurement cameras. Measuring heat transfer by radiation has proven to be very valuable in medicine. One such medical application is the early detection and monitoring of breast cancers. Since tumors cause the rise in local tissue temperature, they can be observed as small embedded heat sources. The focus of this paper is the construction of new artificial test sets for heat source parameter estimation (such as the source depth, volume and intensity/size), to be used before clinical trials. A mixture of ballistic gelatin was used as a heat conductance medium, while a resistor grid (consisting of nine resistors) was used as a heat source, embedded inside the gelatin. Simulation procedure was conducted, resulting in a rank list of parameter configurations for every heat source of the grid. The expected values of parameters were found to be high on the configuration list, with about the first 20% of configurations present in the search space. This paper shows a convenient and effective way of testing parameter estimation methods. On the other hand, although ballistic gelatin presents a homogeneous mixture for heat transfer, with similar density and elastic properties as the living tissue, it does not necessarily have the same thermal conductance. Therfore the possibilities for future development of new materials for comparing parameter estimation methods on artificial test sets should be considered, as well as development of more complex materials consisting of multiple layers and thus more accurately emulating the heat dispersion in human bodies.

INTRODUCTION

Human body is capable of maintaining a constant temperature that is different from that of the surroundings *(1)*. This ability is essential to sustaining a relatively constant environment in the human body, known as homeostasis. Since changes in temperature of the body of more than a few degrees Celsius can disrupt the essential chemical processes in the body, the significance of body temperature as a clear indicator of a bodily dysfunction needs to be noted *(1)*.

Measuring heat transfer by radiation has proven to be of great value in medicine. Most of the thermal radiation that is emitted by an object is located in a small part of the infrared spectrum of electromagnetic radiation (EM radiation), called the *thermal infrared spectrum*, occupying wavelengths from 7 μm to 15 μm *(1)*. Dissipation of thermal radiation can be quantified using *thermal infrared measurement cameras* which

generate images that represent the distribution of thermal infrared radiation on the surface of an object.

Changes in the tissue, such as tumors or inflammations, can influence the temperature of the skin. Diagnosis and monitoring of breast tumors has already been researched to a great extent. The temperature conditions in breast cancer have first been evaluated by Lawson and Gaston. They found that every mammary carcinoma was warmer than its arterial blood supply because of the venous drainage from the tumor *(2)*. Heat propagation from the tumor to the surface of the body can cause local rise in the skin temperature for up to a few degrees Celsius.

Thermal images (thermograms), although used for inflammation detection and skin temperature symmetry assessment, have also been used in attempts to estimate the parameters of embedded tumors (such as their depth, size, blood perfusion, etc.). Approaches have mostly been based on creating a hemispherical 2D or 3D computational models of the breast and performing finite element analysis as described in *(3, 4)*, the use of machine learning techniques *(5, 6)* or creating more realistic models of the breast (i.e. by applying gravity deformations to a hemispherical model) *(7)*.

The work described in this paper is based on the simulation method explained in our previous study *(8)*, where a 3D thermographic imaging device was used to obtain *ad hoc* 3D models of every test subject. This provides for the most accurate data source for individual modeling of the heat dispersion through human body regardless of the method utilized for parameter estimation. The simulation from *(8)* is applicable in analysis of breast and other types of tumors under consideration that it is possible to simplify and assume that a tumor can be approximated with a point heat source. Also, a 4D thermography system described in *(9)* has been considered for data acquisition. However, it did not provide high enough resolution and accuracy for this application.

This paper focuses on the construction of a new experimental test set for heat source parameter estimation, as well as its application in performing the simulation process and result analysis. The aim of this study was to create a homogeneous ballistic gelatine mixture with a number of embedded heat sources, intended to provide an easier and more systematic approach to verification of a parameter estimation method. Concretely, in this work, the simulation method described in *(8)* was verified using the created experimental set.

MATERIAL AND METHODS

An experiment was conducted in order to collect the data required for algorithm development and verification. A homogeneous mixture of ballistic gelatin was used as a medium for heat transfer, while the heat source was constructed in the form of a 3×3 matrix of resistors. What follows is the detailed description of the created test set, as well as methods used for image acquisition and analysis.

Heat source resistor grid

According to Joule's law, the heat generated by the current flowing through the conductor is proportional to the square of the current (I^2), and can be expressed as:

$$Q = I^2Rt[\mathrm{J}] \quad (1)$$

where Q is the heat generated by the current I flowing through the resistance R during the time t. Since the generated heat is proportional to the current and resistance, by changing these values the temperature of a resistor can effectively be regulated. Therefore, a resistor can be used as a single compact heat source. The heat source used for experimental measurements in this study consisted of nine resistors, positioned in a 3×3 matrix, as shown in Figure 1. Resistors were connected to a switch which was used for selection of a single resistor as the net load. By choosing a resistor, the current was passed through it, causing the resistor to heat up to a constant temperature after some warm up time t. All resistors were of the same nominal value, thus approximately generating the same ammount of heat.

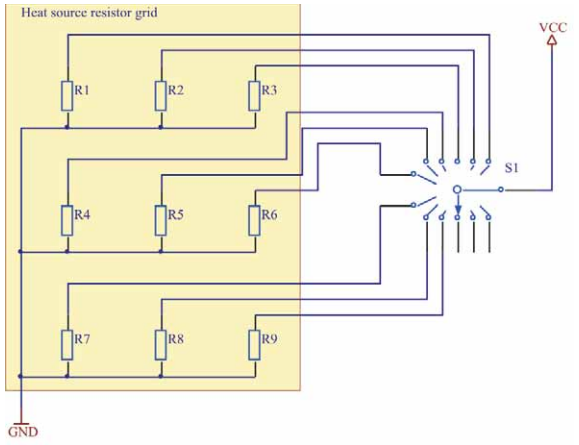

Figure 1. *The reistor grid used as a grid source during experimental data collection.*

Figure 2. *Ballistic gelatin with embedded heat source grid and external resistor selector.*

Heat transfer medium

In order to emulate (simplified) realistic conditions of heat transfer, specifically in the modeling of the human breast, a homogeneous mixture was created. The mixture's composition is similar to the composition of the ballistic gelatin described in *(10)*, although some modifications were applied. The ballistic gel was prepared with about 30% gelatin to water ratio, compared to the 20% mixture described in *(10)*. The reason for the increased ratio was to make the mixture denser since it had to be used at room temperature and thus could not be cooled to 4°C. In addition, a small amount of preserving agent was added to the mixture to slow down its degradation and delay the spoiling of the mixture.

Upon completion of the ballistic gelatin, it was poured into a hemispherical rubber mould of radius of 6.5 cm, with the heat source grid placed inside. The resulting composition is shown in Figure 2.

Geometric and thermal data acquisition

Geometric and thermal data of the ballistic gelatin were acquired using the 3D thermography system described in *(11)*. The system consisted of an active 3D scanner used for object surface reconstruction, based on a digital light processing (DLP) projector and a RGB (Red-Green-Blue) camera, while the surface temperature is measured and recorded using a thermal measurement camera. The 3D scanner utilizes the structured light method of scanning. A series of light patterns, such as vertical or horizontal stripes, concentric rectangles, etc., were projected onto the object's surface. Pattern contours were recorded with the RGB camera and processed on a computer to produce 3D models of the scanned object.

The ballistic gelatin was placed in a fixed position during the acquisition process. Geometric structure was reconstructed only once, while its surface temperature distribution was measured for every heat source in the grid. Before every temperature acquisition, the ballistic gelatin was first cooled down to the room temperature. Afterwards, a single resistor from the grid was activated. When the surface temperature stabilized, thermal image of the gelatin was taken. The 3D scanning procedure is shown in Figure 3, while Figure 4, Figure 5 and Figure 6 show the 3D model, corresponding thermal image when resistor 2 was active, and the complete 3D thermogram, respectively.

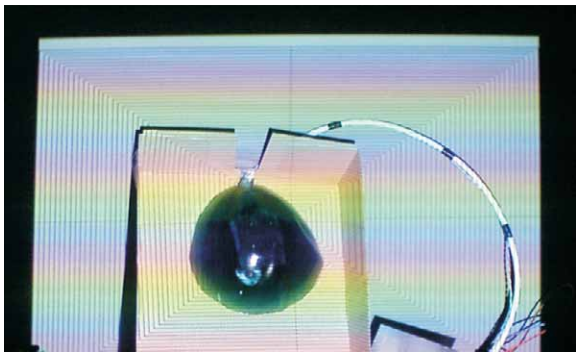

Figure 3. *Scanning the surface of the ballistic gelatin.*

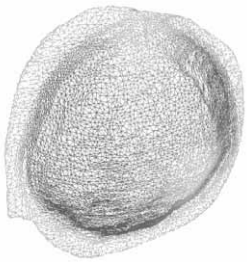

Figure 4. *The scanned 3D model of the ballistic gelatin.*

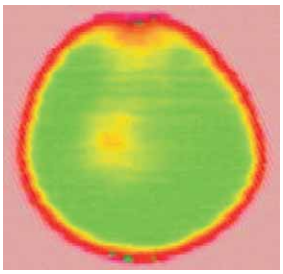

Figure 5. *Thermal image of the ballistic gelatin when resistor 2 was active.*

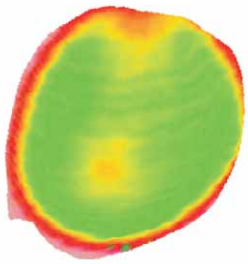

Figure 6. *The 3D thermogram of the ballistic gelatin when resistor 2 was active.*

Data processing and simulation

Data processing and simulation procedure were conducted as described in our previous study *(8)*. Thermal images obtained by the thermal measurement camera were converted to grayscale, using the per-segment interpolation model explained in *(8)*. The model is composed of four line segments, spanning through five colors: blue, cyan, green, yellow and red, as shown in Figure 7.

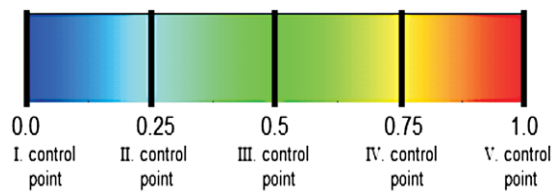

Figure 7. *Color interplation between line segments in RGB space.*

A single number from the range [0,1] is assigned to the temperature measured at every pixel. This value represents the relative temperature from one pixel to the others, and is calculated by determining the line segment in the color space closest to the pixel's color, and finding the parameter t of the point on that line segment that is closest to the pixels color. The parameter t is the parameter of the line equation as shown by (2):

$$x_0 = x_1 + t \cdot (x_2 - x_1) \tag{2}$$

where x_1 and x_2 are the points that define the line, i.e. its start and end points respectively, and x_0 is an arbitrary point on that line. In this case, x_0, x_1 and x_2 represent points of a line in the RGB color space. Parameter t is then scaled so that it fits the range shown on Figure 7.

For the purpose of simplification, in this paper a heat source was approximated as a radiant point source. Heat source parameters were estimated using the simulation method described in *(8)*. These parameters include the heat source depth, size and intensity. An example of application of such estimation procedures includes estimating the parameters of an embedded tumor from thermal images. A great amount of research has been focused on the analysis of human breast tumors, as mentioned in the Introduction section. Unlike other methods that produce a single estimated solution *(5, 6, 12)*, simulation model used in this study produces a rank list of most likely configurations of parameters (conformations) that describe the heat source. Each conformation is scored with the total difference of the measured surface temperature and the temperature distribution determined by that conformation. The Gaussian function is used as the radiant function, as shown in equation (3):

$$f(x) = A \cdot e^{\frac{|x-\mu|^2}{2\sigma^2}} \tag{3}$$

where parameter A corresponds to the maximum temperature of the heat source, μ to the distance from the heat source to the point of the local thermal maximum on the surface of the observed object, and σ is proportional to the intensity (or size) of the heat source. It is important to note that additional experiments have to be conducted in order to obtain an accurate physical representation of the parameter σ.

Given these three parameters, the value of the radiant function can be determined at any value x. Concretely, x is the position of a vertex on the surface of the scanned 3D object, while $|x - \mu|$ is the distance from that vertex and the center of the Gaussian function (determined by depth parameter μ). For any set of parameters μ, σ and A the radiant function is evaluated at every vertex of the 3D object, and then used as the monochromatic color value of the corresponding vertex. The resulting gray-scale colored model is used as the simulated temperature distribution for a specific conformation, and is afterwards compared to the actual measured temperature distribution. Greater details on the simulation process can be found in *(8)*.

While the values of parameters in the real-world coordinate space are measured in centimeters (μ_{cm}, σ_{cm}) and degrees of Celsius (temperatures), their corresponding values in the simulation space, μ_{sim}, σ_{sim} and A_{sim}, are expressed without units. The relationship between these two sets of parameters is shown by equations (4), (5), (6) and (7).

$$\mu_{sim} = \frac{l_{sim}}{l_{cm}} \mu_{cm} = k \cdot \mu_{cm} \tag{4}$$

$$A_{sim} = 1.0 + \frac{T_{heat_{source}} - T_{scale_{max}}}{T_{scale_{max}} - T_{scale_{min}}} \tag{5}$$

$$f_{sim}(x) = A_{sim} \cdot e^{-\frac{|x-\mu|^2}{2\sigma_{sim}^2}} \tag{6}$$

$$\sigma_{sim}^{\ 2} = -\frac{|x - \mu_{sim}|^2}{2ln\frac{f_{sim}}{A_{sim}}} \tag{7}$$

Here, l_{cm} is the distance between two reference points in real-world coordinate space, l_{sim} the distance between those same two points in the simulation's 3D space, and $f_{sim}(x)$ the value of the radiant function in the simulation space, for a given parameter x. Since the coordinates in simulation space are expressed without units, the values of parameters μ, σ, A and l are also unit-less in simulation space. The value A_{sim} was calculated once for every heat source, and was afterwards held fixed during the simulation (although searching through the space of amplitudes is also possible in the implemented simulation). A_{sim} represents the maximum amplitude of the Gaussian function in its center, scaled using the temperature range covered by the thermal camera. Parameters needed to calculate A_{sim} are the temperature of the heat source measured when the source was outside the ballistic gelatin, and maximum and minimum temperature displayable by the thermal measurement camera $T_{heat_{source}}$ and $T_{scale_{min}}$, respectively.

RESULTS

Measurements of temperatures of nine separate heat sources were performed twice. Initially, temperature measurements of each resistor were conducted prior to submersing the resistor grid into the ballistic gelatin. The average of the measured temperatures was 41.03°C, with standard deviation of 0.55°C. Since resistors $R_1 - R_9$ are of the same nominal value, the variations in temperatures are assigned mostly to the angle between every resistor and the thermal measurement camera, and inaccuracies in resistances of the elements compared to their nominal values. These maximum values of resistor temperatures are used as a reference during the simulation process.

The second measurement was conducted after the resistor grid was placed inside the gelatin. Separate heating of every resistor was repeated, and the temperature distri-

bution of the ballistic gelatin recorded. Due to measurement errors, data related to resistor 9 had to be discarded from the analysis process. The resulting grayscale 3D thermograms of the ballistic gelatin, with active resistors 2, 4 and 7, are shown in Figure 8, Figure 10 and Figure 12, respectively. Only three test cases are presented, since the analysis process is analogous for the rest of the obtained data set.

Once temperature measurements were conducted, the depth of every resistor from the surface of the ballistic gelatin was determined. The depth was measured by creating a puncture perpendicular to the gelatin surface above each resistor using a needle, and measuring its insertion length. The measured depths of resistors 2, 4 and 7 are shown in Table 5.

Figure 9, Figure 11 and Figure 13 show renderings of a single resulting conformation for the simulations on the data obtained from the ballistic gelatin while resistors 2, 4 and 7 were active, respectively.

Ranges of parameters used in simulation of the heat produced by resistors 2, 4 and 7 are given in Table 1. Parameter μ represents the depth of the heat source in the simulation's coordinate space. Maximum value of μ was set to be equal to the thickness of the ballistic gelatin scaled by the size ratio of the simulation-space 3D coordinates and the real-world coordinates as shown by equation (*4*). Scaling ratio was been calculated by comparing distances of several reference points in both simulation and real-world coordinate spaces. The range of σ has been chosen experimentally, while A represents each resistor's maximum temperature value scaled to the tem-

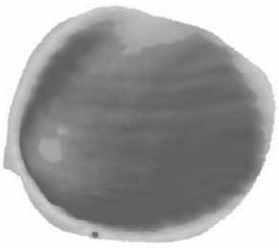

Figure 8. *Grayscale 3D thermogram of the ballistic gelatin with resistor 2 active.*

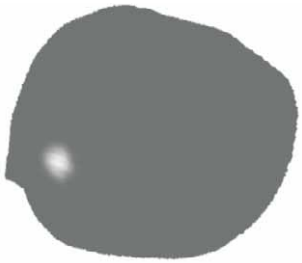

Figure 9. *Simulation result for configuration 113 from Table 2.*

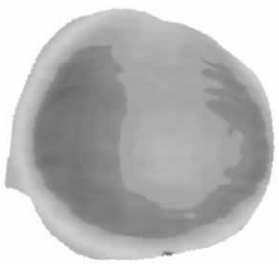

Figure 10. *Grayscale 3D thermogram of the ballistic gelatin with resistor 4 active.*

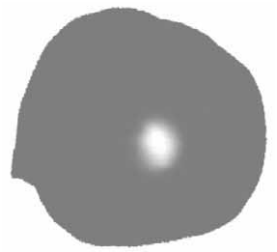

Figure 11. *Simulation result for configuration 262 from Table 3.*

Figure 12. *Grayscale 3D thermogram of the ballistic gelatin with resistor 7 active.*

Figure 13. *Simulation result for configuration* 351 *from Table 4.*

TABLE 1

Ranges of parameters in the search space used in the simulation. The table shows parameters for active resistor heat sources 2, 4 and 7.

Parameter	Source 2		Source 4		Source 7	
	min	max	min	max	min	max
μ	0.03	6.50	0.03	6.50	0.03	6.50
σ	0.01	0.40	0.01	0.40	0.01	0.40
A	6.17	6.17	4.48	4.48	6.17	6.17

TABLE 2

Selected results of the simulation for heat source 2.

Rank	Heat source parameters		
	μ	σ	A_{max}
113	0.17 (≈ 1.30 cm)	0.12	6.175
158	0.13 (≈ 1.00 cm)	0.09	6.175
159	0.17 (≈ 1.30 cm)	0.11	6.175
Expected	≈ 0.13 (≈1.00 cm)	≈ 0.10	(fixed)

TABLE 3

Selected results of the simulation for heat source 4.

Rank	Heat source parameters		
	μ	σ	A_{max}
245	0.20 (≈ 1.53cm)	0.14	4.482
256	0.21 (≈ 1.61cm)	0.17	4.482
262	0.19 (≈ 1.46cm)	0.15	4.482
Expected	≈ 0.19 (≈1.40cm)	≈ 0.16	(fixed)

TABLE 4

Selected results of the simulation for heat source 7.

Rank	Heat source parameters		
	μ	σ	A_{max}
324	0.14 (≈ 1.08 cm)	0.13	6.175
336	0.12 (≈ 0.92 cm)	0.13	6.175
351	0.11 (≈ 0.85 cm)	0.13	6.175
Expected	≈ 0.12 (≈ 0.90 cm)	≈ 0.13	(fixed)

TABLE 5

Measured depths of the resistors within the ballistic gelatin.

Resistor No.	Depth (cm)
2	1.0
4	1.4
7	0.9

perature span provided by the thermal measurement camera. The simulation is performed with step size of 0.01 for every parameter in the search space. The number of conformations recorded for the case when resistor 2 was active is equal to 1568, for resistor 4 to 1750, and for resistor 7 to 1803. Some sensible conformations of parameters, which have values of μ_{sim} close to the measured depth converted to simulation space coordinates and σ_{sim} to the value calculated using equation (6) with measured temperatures of heat sources and the object surface, are shown in Table 2, Table 3 and Table 4. These conformations rank in the first 10.1%, 20.0% and 19.5% of the highest scored conformations for each resistor, respectively.

Score estimates of all conformations in the search space were calculated, and the results of the simulation process are given in the form of a sorted list. Examples of conformations that provide a good parameter estimate for parameters of heat sources 2, 4 and 7 are given in Table 2 – Table 4. In Table 5, the actual measurements of resistor depths are given.

CONCLUSION

The use of ballistic gelatin enables easy design of homogeneous materials of desired shape and density. In this paper, a hemispherical object consisting of ballistic gelatin and an embedded heat source resistor grid was constructed. Since the created gelatin is of hemispherical shape and the resistor grid is mounted on a flat circuit board, placing the grid inside the gelatin causes the resistors to have varying depths from the surface. This has shown to be a simple and effective method for testing the simulation, and determining the parameters of multiple heat sources.

The advantage of such an approach is in its simple construction and easy real-world parameter measurements. Measuring the depth of the resistors can be conducted by puncturing the ballistic gelatin above a resistor using a needle and determining its insertion length, while the temperatures of resistors prior and after their immersion in the gelatin can be performed using the thermal measurement camera. These measurements are later used as the reference values for the results of the simulation process.

Although providing the possibility to approximate some physical properties of human or animal tissues, such as their density and elasticity, ballistic gelatin does not necessarily have the same thermal conductivity as living tissue. Also, since the mixture is homogeneous, it does not compensate for the differences in the tissue, such as the vascular and nervous systems, but represents the average tissue properties.

Verification of the heat dispersion simulation method described in *(8)*. was performed. The simulation yielded the expected results within the first 20% of the conformation rank lists for all three analyzed cases. The results of the simulation are satisfactory, although still providing enough room for its future improvements. Since the aim of this study was to provide experimental test sets for verification of parameter estimation methods, as was the one conducted, the applicability of the solution based on ballistic gelatin was confirmed through this example.

Future work should be focused on the following steps. New homogeneous physical models should be constructed in order to additionally test and improve the simulation method. Also, experiments with non-homogeneous materials should be conducted, thus providing more accurate information and results. The material

could be designed to be multi-layered, each layer mimicking the thermal properties of the corresponding tissue. One example of such tissue is the human breast which is composed of four main layers: skin, fat tissue, gland and muscle *(4)*.

Finally, upon completion of the aforementioned testing, this simulation could be used in various applications, including medical thermography of the human breast. As mentioned in the *Introduction* section, tumors cause the rise in temperature of the surrounding tissue for up to several degrees Celsius, and can be detected with 2D thermography in a great number of cases. The method utilized in this study can then be used in an attempt to estimate the parameters of the tumor, such as its depth and volume.

Acknowledgment: *The authors acknowledge the support of scientific research project »Methods of scientific visualization» (098-098 2562-2567), founded by the Ministry of Science, Education and Sports of the Republic of Croatia.*

REFERENCES

1. DIADIKES N A, BRONZINO J D 2008 »Medical infrared imaging«. Taylor & Francis Group, LLC.
2. LAWSON R N, GASTON J P 1964 »Temperature measurements of localized pathological processes«. Thermography and its Clinical Applications, Annals of the New York Academy of Sciences, Vol. 121, p 90–98
3. NG E Y-K, SUDHARSAN N M 2004 »Computer simulation in conjuction with medical thermography as an adjunct tool for early detection of breast cancer«. *BMC Cancer 4:* 17
4. LIN Q J, YANG H Q, XIE S S, WANG Y H, YE Z, CHEN S Q 2009, »Detecting early breast tumour by finite element thermal analysis«. *Journal of Medical Engineering and Technology 33(4):* 274–80
5. XU A, YANG H Q, YE Z, SU Y, XIE S 2009, »An approach to parameters estimation for breast tumour by finite element method«. Proceedings of SPIE 7171
6. MITAL M, PIDAPARTI R M 2008, »Breast tumor simulation and parameters estimation using evolutionary algorithms«. Modelling and simulation in engineering, Volume 2008 (2008)
7. JIANG L, ZHAN W, LOEW M H 2011, »Modeling static and dynamic thermography of the human breast under elastic deformation«. *Physics in Medicine and Biology 56:* 187
8. SOVIĆ I, LIPIĆ T, GJENERO L, GRUBIŠIĆ I, SKALA K 2011 »Heat source parameter estimation from scanned 3D thermal models«. Proceedings Vol. I. MEET&GVS 34th International Convention MIPRO, p 252–256
9. SKALA K, LIPIĆ T, SOVIĆ I, GJENERO L, GRUBIŠIĆ I 2011, »4D thermal imaging system for medical applications«. *Period biol 113(4):* 407–416
10. NICHOLAS N C, WELSCH J R 2004 »Ballistic gelatin». Institute for Non-Lethal Defense Technologies, Report.
11. GJENERO L, GRUBIŠIĆ I, LIPIĆ T, SOVIĆ I, SKALA T 2011 »Active 3D scanning based 3D thermography system and medical applications«. Proceedings Vol. I. MEET&GVS 34th International Convention MIPRO, p 269–273
12. QI H, KURUGANTI P T, LIU Z 2002 »Early detection of breast cancer using thermal texture maps«. IEEE International Symposium on Biomedical Imaging, p 309–312